Decoding Lusichelins A-E: An In-Depth Look at the Metallophores of *Lusitaniella coriacea* LEGE 07167 – Structure, Production, and Functionality

Maria Lígia Sousa[1], Leonor Ferreira[1,2], Dora Ferreira[1], Abel M. Forero[3], Raquel Castelo-Branco [1,2], Nikoletta Szemerédi[4], Gabriella Spengler[4], Jaime Rodríguez[3], Carlos Jiménez[3], Pedro Nuno Leão[1], Vitor Vasconcelos[1,2], Mariana Alves Reis[1,*]

[1] CIIMAR/CIMAR, Interdisciplinary Centre of Marine and Environmental Research, University of Porto, Matosinhos, Portugal
[2] Departamento de Biologia, Faculdade de Ciências, Universidade do Porto, Rua do Campo Alegre, Edifício FC4, 4169-007 Porto, Portugal.
[3] CICA - Centro Interdisciplinar de Química e Bioloxía e Departamento de Química, Rua As Carballeiras, Campus do Elviña, Universidade da Coruña, 15071, A Coruña, Spain
[4] Department of Medical Microbiology, Albert Szent-Györgyi Health Center and Albert Szent-Györgyi Medical School, University of Szeged, Semmelweis utca 6, 6725 Szeged, Hungary

Essential trace metals are vital for cellular processes such as respiration, DNA replication, and photosynthesis. Cyanobacteria must tightly regulate metal homeostasis to prevent deficiency or toxicity, yet their metallophores remain overlooked. Here, we report lusichelins A-E (**1-5**), new metallophores isolated from the marine cyanobacterium *Lusitaniella coriacea* LEGE 07167. Their structures and configurational assignments were determined using NMR, mass spectrometry, TD-DFT calculations, and retrobiosynthetic insights. Lusichelins feature a unique structural arrangement with thiazoline/thiazole rings connected by a vinyl group, an aliphatic carbon chain, or directly, enabling potential for hexadentate metal coordination. Genomic analysis identified a hybrid PKS/NRPS biosynthetic gene cluster consistent with the structure of lusichelins and bearing traits characterisitic of metallophore biosynthesis. Notably, lusichelin production was influenced by salt composition in the culture medium rather than iron availability, suggesting an atypical regulatory mechanism. Functionally, lusichelins acted as copper detoxifiers, and lusichelin B (**2**) exhibited cytotoxicity against colon carcinoma cells while reversing multidrug resistance via ABCB1 efflux pump modulation. These findings expand the understanding of cyanobacterial metallophores in microbial metal homeostatis and highlight their potential in biological applications

Introduction

Cyanobacteria, ancient photosynthetic microorganisms, have thrived for over 3.5 billion years, inhabiting diverse ecosystems ranging from marine and freshwater habitats to extreme environments such as deserts, hot springs, and metal-contaminated areas.[1,2] This remarkable ecophysiological diversity is mirrored in their metabolic plasticity, highlighting their value in drug discovery. Cyanobacteria have contributed to the development of four approved anticancer drugs, with numerous other secondary metabolites recognized for their unique structures and diverse bioactivities.[3] As photoautotrophs, cyanobacteria have a particularly high demand for metals, as these micronutrients serve as cofactors in numerous proteins involved in respiration and photosynthesis. However, excess metals can disrupt these critical processes, necessitating sophisticated mechanisms to maintain metal homeostasis. In cyanobacteria, these include producing extracellular polymeric substances, synthesizing metallothioneins, activating metal transporters and excreting metallophores.[2,4,5]

Siderophores, a well-studied class of metallophores, are low molecular weight metabolites that reversibly bind Fe(III) as a hexadentate octahedral complex, facilitating its cellular uptake via specific receptors. Their production is generally influenced by the iron requirements of the organism and the availability of iron in the local environment.[6] Based on their chemical structure, these iron chelators can be classified as hydroxamates, catecholates/phenolates, α-hydroxy carboxylates, or mixed type.[6–8] Compared to other microbial siderophores, knowledge of

cyanobacterial siderophore diversity and role is still limited.[4,9] Those that have been reported were isolated from iron-limited cultures and belong either to the hydroxamates, such as schizokinen [10] and synechobactin A [11], or to the catecholates, including anachelin H [12] and cyanochelin A [13]. Recent advances on the genome mining tools allow for the detection of signature genes responsible for specific metallophore biosynthesis, such as those from non-ribosomal peptide synthetases (NRPS) or NRPS-independent synthetases. These genes are often found in biosynthetic gene clusters (BGCs) alongside with metallophore transport and regulatory genes, such as TonB transporters and AraC transcriptional regulators.[14,15] Given the biosynthetic potential of cyanobacteria, together with these specific detection tools [16], many of the unknown cyanobacterial metallophores are sure to be brought to light in the near future.

During our bioactivity-guided discovery program, using untargeted metabolomics, we identified the filamentous marine cyanobacterium *Lusitaniella coriacea* LEGE 07167 as a potential producer of novel cytotoxic compounds[17]. This discovery prompted a deeper investigation into this strain, leading to the characterization of lusichelins A-E (**1-5;** Fig. 1), a new group of cyanobacterial metallophores. The putative BGC identified in this strain includes transport and regulator gene signatures consistent with metallophore biosynthesis and compatible with the proposed structures. Culture experiments showed the multifunctional role of lusichelins as both siderophores and copper detoxifiers. We hypothesize that lusichelin C (**3**) serves as primary metallophore, with lusichelins A (**1**) and B (**2**), carboxylate forms of **3**, serving as cellular reservoirs. Furthermore, we confirmed the previously observed bioactivity [17], with lusichelin B (**2**) demonstrating stereospecific cytotoxic activity against human colon cells and modulation of efflux pumps related to cancer multidrug resistance. Our study not only increase the known diversity of cyanobacterial metallophores but also provides insights into their multifunctional roles in metal homeostasis and cytotoxicity.

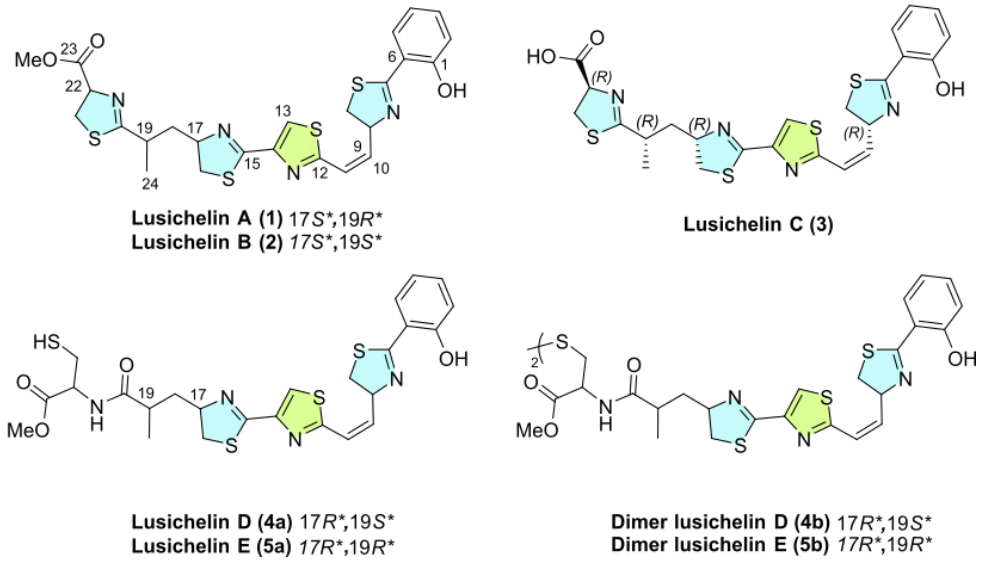

Fig. 1 Structures of lusichelins A-E (**1-5**) isolated from *Lusitaniella coriacea* LEGE 07167

Results and discussion

Isolation and structural elucidation of the planar structure of lusichelins A-D (1-5)

In our previous bioprospecting project involving several cyanobacteria from the LEGE-CC collection [17], we identified *Lusitaniella coriacea* LEGE 07167 as a potential producer of novel secondary metabolites. Through molecular network analysis using GNPS (Global Natural Products Social Molecular Networking) platform[18], we discovered a unique cluster in this strain, domposed of five mass features that could not be dereplicated. After culture scale-up of the producing cyanobacterium, mass-guided isolation (SI Fig. S1), involving several normal and reverse-phase chromatographic steps, yielded lusichelins A-E (**1-5,** Fig. 1).

The molecular formula of **1**, ($[\alpha]_D^{23}$ +202.2), $C_{25}H_{26}N_4O_3S_4$, was deduced from the $[M+H]^+$ protonated ion observed in its (+)-HRESIMS at *m/z* 559.0964, (calcd for $C_{25}H_{27}N_4O_3S_4$, *m/z*

559.0961), indicating the presence of 15 degrees of unsaturation. Strong infrared absorption bands at 3400 and 1742 cm^{-1} suggested the presence of hydroxyl and ester carbonyl functionalities, respectively.

The ^{1}H and ^{13}C NMR data of **1**, combined through HSQC-edited experiments, allowed the identification of 25 carbon resonances, which were assigned to two methyl groups, four methylenes, four aliphatic and seven olefinic methines, and eight sp^2 non-protonated carbons (SI Table S1). The presence of three thiazoline rings in **1** was inferred from an HMBC experiment. Three sets of long-range correlations were observed: 1) from δ_H 4.14/3.19 (H8a/H8b) and 6.32 (H9) to δ_C 172.8 (C7); 2) from δ_H 3.48/3.03 (H16a/H16b) and 4.72 (H17) to δ_C 161.8 (C15); and 3) from δ_H 3.55/3.51 (H21a/H21b) and 5.11 (H22) to δ_C 179.6 (C20) were assigned respectively to the presence of thiazoline moieties (**A**, **C** and **D** rings in Fig. 2A). The presence of a thiazole ring (**B** ring

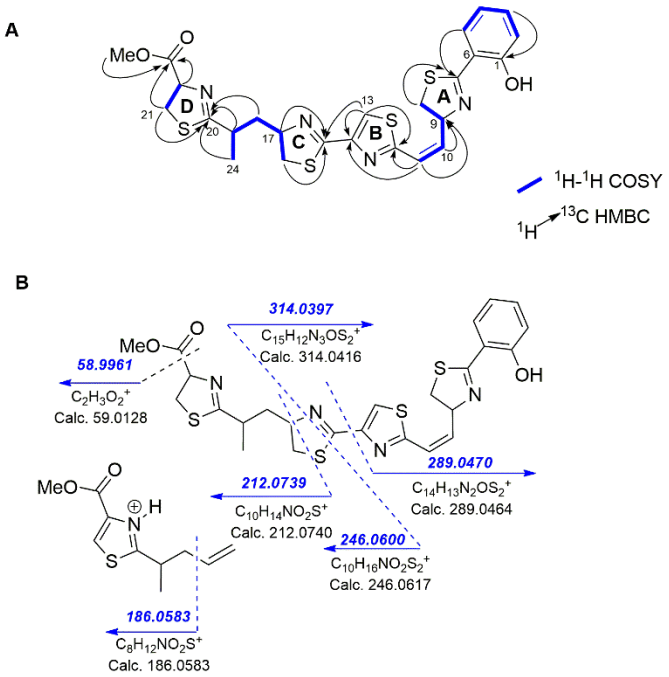

Fig. 2 Structural determination of lusichelins A and B (**1-2**). (A) Four independent ^{1}H-^{1}H spin systems (highlighted in bold blue) deduced from their 1H-^{1}H COSY spectra were connected by key HMBC correlations (indicated by black arrows). (B) MS^2 fragmentation pattern with major ions annotated (*m/z*) deduced from the (+)-HRESIMS/MS analysis

in Fig. 2A) was also deduced from the HMBC cross-peaks between the non-protonated sp^2 carbons at δ_C 163.2 (C12) and 150.5 (C14) and the sp^2 methine proton at δ_H 7.97 (s, H13). Furthermore, the ^{1}H-^{1}H COSY experiment revealed four isolated spin systems that were connected by heteronuclear-^{1}H-^{13}C HMBC correlations (Fig. 2A).

The ^{1}H NMR spectrum of **1** displayed characteristic signals of four aromatic protons at δ_H 7.47-6.89, whose splitting pattern and coupling constants (*ortho J* = 7.3 and 8.5 Hz, *meta J* = 1.2 and 1.6 Hz) were indicative of an *ortho*-disubstituted benzene ring. The broad singlet at δ_H 12.63 observed in the ^{1}H NMR spectrum of **1**, suggested the presence of an *ortho*-substituted phenol ring. This *ortho*-phenol moiety was connected to the first thiazoline (**A** ring), through a long-range correlation between the imine carbon at δ_C 172.2 (C7) to the aromatic proton H5 (δ_H 7.47 dd), suggesting the presence of a salicyl-thiazoline moiety. This assignment was further confirmed by comparison with compounds such as piscibactin[19] and amamistatin[18], bearing a similar fragment. Key ^{1}H-^{1}H COSY correlations were observed between methylene protons at δ_H 4.14 and 3.19 (H8a/H8b) and methine proton at δ_H 6.32 (H9) of the thiazoline **A** ring, and the olefinic protons H10 (δ_H 6.25), and H11 (δ_H 6.62). Additionally, an HMBC correlation was observed between the olefinic proton H11 and the thiazole carbon at C12 (δ_H 163.2). These ^{1}H-^{1}H COSY and HMBC correlations established the connectivity between the thiazoline **A** and the thiazole **B** rings through the $\Delta^{10,11}$ olefin linkage. Likewise, the ^{1}H-^{1}H spin system from methylene H16 to the methyl H24, and the long-range proton-carbon correlation between H19 (δ_H 3.22), H21 (δ_H 3.55/3.52), and H24 (δ_H 1.32) to C20 (δ_C 129.6) allowed us to connect the second to the third thiazoline (**C** and **D** rings, respectively) through a $CH(CH_3)CH_2$ group (Fig. 2A). Thiazole **B** and thiazoline **C** rings were connected through C14 and C15 carbons based on an HMBC correlation

from H13 (δ_H, s, 7.97) to C15 (δ_C 161.8). Finally, a methoxycarbonyl group (δ_H 3.80 s; δ_C 52.9 (C25)) and 171.5 (C23) was linked to the position C22 of the thiazoline **D** ring by the HMBC correlation between C23 (δ_C 171.5) and H22 (δ_H 5.11). The 1D and 2D NMR data (SI Fig. S2-S6) allowed us to establish the planar structure of **1**, named as lusichelin A, which was also supported by the mass fragmentation pattern displayed in its (+)-HRESIMS/MS (Fig. 2B).

The (+)-HRESIMS of **2** ($[\alpha]_D^{23}$ +152.4) displayed a $[M + H]^+$ ion adduct at *m/z* 559.0964, indicating that it is an isomer of **1**. Furthermore, NMR data of **2**, named as lusichelin B, were very similar to those of **1** (SI Table S1; SI Fig. S10-S14), except for the chemical shifts at positions C17, C18, C19, and C24 ($\Delta\delta_C$ > 0.5 ppm). These differences suggested a distinct configuration at C17 or C19 stereocenters between **1** and **2** (see below).

Compound **3**, named as lusichelin C, ($[\alpha]_D^{24}$ + 431.3; yellow amorphous powder) showed a prominent $[M+ H]^+$ ion adduct in its (+)-HRESIMS at *m/z* 545.0803 (calcd. for $C_{24}H_{25}N_4O_3S_4$ *m/z* 545.0804), indicating a molecular formula of $C_{24}H_{24}N_4O_3S_4$. Given the similarity of ^1H an ^{13}C NMR data for **3** to those of **1** and **2**, an analogous assignment strategy was used to elucidate its structure (SI Table S1; SI Fig. S17-S23). The mass difference of 14.0157 Da between the molecular formula of **3** to that of **1** or **2,** suggested the absence of a methyl group in **3**. This was confirmed by the lack of proton and carbon chemical shifts in the NMR spectra of **3** corresponding to a methoxy group present in **1** and **2**. All these data indicated the presence of a carboxylic acid functionality in **3** (δ_{C23} 174.5) instead of the methyl ester group present in **1** and **2** (SI Table S1).

The molecular formula of **4a** was established as $C_{25}H_{28}N_4O_4S_4$, on the basis of its (+)-HRESIMS that display the $[M+H]^+$ ion at *m/z* 577.1069 (calcd for $C_{25}H_{29}N_4O_4S_4$ *m/z* 577.1066). Comparison of the molecular formula of **4a** to that of **1** and **2** indicated that **4a** has OH_2 additional atoms (Δ 18.0105 Da). The ^1H and ^{13}C NMR data of **4a** from position C1 to C19 (SI Table S1) were identical to those of **1** and **2**, suggesting that **4a** has the same salicyl-thiazoline fragment connected through a disubstituted *Z*-olefin to a thiazole-thiazoline moiety and this is in turn to a -$CH(CH_3)CH_2$- group. The main carbon and proton chemical shift differences between the NMR spectra of **1**/**2** and **4a** were observed at positions C21 and C22. The observed differences, along with the presence of additional OH_2 atoms, suggested that the thiazoline ring D in **4a** might be opened. This proposal was supported by the spin system observed in the ^1H-^1H COSY of **4a** displaying correlations among the amide proton at δ_H 6.96 (d, *J* = 7.8 Hz), the methine H22 (δ_H 4.95 dt/ δ_C 53.7), and the methylene H21 (δ_H 3.07 and 2.99/ δ_C 27.2). The characteristic ^1H and ^{13}C NMR chemical shift values of α- and β-carbons of a methylester cysteine moiety for C22 and C21 (SI Table S1) and those corresponding to a methoxy group at δ_C 53.0/ δ_H 3.80 agree with the presence of an opened thiazoline ring D bearing a methylester in **4a**. Moreover, the HMBC cross-coupling from H21 to the carbonyl group at C20 (δ_C 175.7) allowed us to link the methylester cysteine moiety to the C1-C19 fragment through an amide functionality. The 14 degrees of unsaturation present in **4a,** instead of the 15 degrees in **1** and **2,** agree with the presence of an opened thiazoline ring in **4a**. Interestingly, the NMR spectra of **4a** displayed additional chemical shifts that suggested that **4b** was isolated along with itssulfide dimer, compound **4b**. The presence of **4b** was deduced by the sequential proton-proton cross peaks of an amide proton at δ_H 7.04 (d, *J* = 7.8 Hz) with a methine H22 (δ_H 4.86/ δ_C 51.6) and methylene H21 (δ_H 3.18/δ_C 40.3) observed in a ^1H-^1H COSY experiment. LC/HRESIMS analysis confirmed the presence of the sulfide dimer **4b** (SI Fig. S35). Indeed, the HPLC chromatogram displayed **4a** at R_t 4.33 min along with another chromatographic peak at R_t 13.88 min corresponding to **4b** which (+)-HRESIMS showed a $[M+Na]^+$ ion adduct at *m/z* 1173.1721 (calcd *m/z* 1173.1722 for $C_{50}H_{54}NaN_8O_8S_8$) and a doubly charged ion at *m/z* 576.0986 $[M+H]^{2+}$. A 1:0.8 between ratio between the monomer **4a** and the sulfide dimer **4b** was deduced from the ^1H NMR spectrum. Compounds **4a** and **4b** were named as lusichelin D and dimer lusichelin D, respectively. The isomeric structure between **5a** and **4a** was proposed from the $[M+ H]^+$ ion adduct displayed at *m/z* 577.1069 in the (+)-HRESIMS of **5a**. Also, the NMR spectral data of **5a** were very similar to those of **4a** (SI Table S1) but differing in the chemical shifts at positions C17 and C19, suggesting a different configuration at these stereocenters. The presence of a mixture of the thiol monomer **5a** and its sulfide dimer **5b**, that were called lusichelin E and dimer lusichelin E, respectively, was also deduced from the NMR (SI Fig. S36-40) and LC/HRESIMS data (SI Fig. S41). In this case, the ^1H NMR spectrum displayed a 0.6:1 ratio between the thiol **5a** and its sulfide dimer **5b**. The origin of **4b** and **5b** as extraction or separation artifacts could not be ruled out.

Identification of the putative lusichelins (*lus*) biosynthetic gene cluster

To identify the putative lusichelins biosynthetic gene cluster (BGC), the whole genome of *L. coriacea* LEGE 07167 was sequenced. A combination of short-read Illumina and long-read Nanopore sequencing technologies yielded a draft genome of 5.97 Mb distributed by two contigs (Genbank: JBBBDN000000000). The sequence was analyzed using antiSMASH 7.0 [15], which identified seven BGCs. The only plausible candidate for lusichelins biosynthesis was annotated as a hybrid NRPS/PKS metallophore BGC, encoding four NRPS modules intercalated by type I PKS genes (Fig. 3A). The four NRPS modules contain adenylation domains with predicted specificity for cysteine, as well as heterocyclization domains suggesting the presence of thiazoline/thiazole moieties in the BGC products, which is consistent with the structure of lusichelins A-C (**1-3**). Other significant features encoded within this BGC include a salicylate synthase, metallophore-related transporters, and an AraC transcriptional regulator (SI Table S2). The ATP-binding cassette (ABC) and major facilitator (MFS) superfamilies of transporters, TonB-dependent receptor, and heavy metal translocating P-type ATPase are related to cyanobacterial siderophore export/import

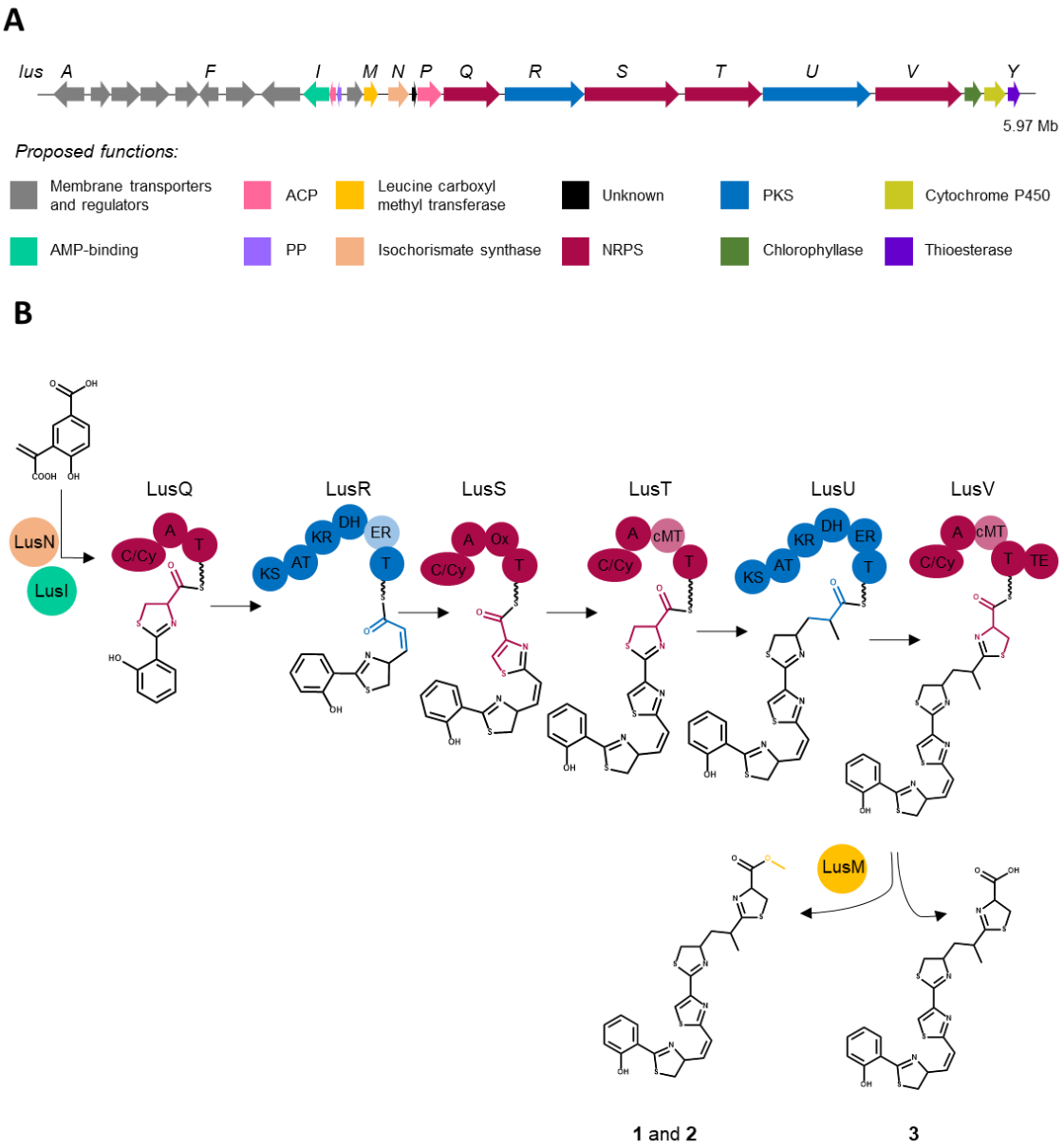

Fig. 3 Proposed biosynthetic pathway of lusichelins in *Lusitaniella coriacea* LEGE 07167. **(A)** Bioinformatics-based annotation of *lus* BGC. ACP (Acyl-Carrier Protein); PKS (Polyketide Synthase); PP (Phosphopantetheinyl transferase); NRPS (Non-Ribosomal Peptide Synthetase) **(B)** Biosynthetic model for lusichelins A-C (**1-3**) assembly along with domain annotation. C/Cy (Condensation/heterocyclization); A (Adenylation); T (Thiolation); KS (Ketosynthase); AT (Acyltransferase); KR (Ketoreductase); DH (Dehydratase); ER (Enoylreductase); Ox (Oxidase); cMT (Carbon methyltransferase); TE (Thioesterase).

systems.[4] Based on these findings, we consider this BGC as the putative lusichelin gene cluster (*lus*) and propose a biosynthetic model for lusichelins assembly (Fig. 3B).

The assembly line for lusichelins mirrors other salicyl-capped siderophore biosynthetic pathways.[7] It is proposed to initiate with the generation and activation of salicylate: LusN, a putative bifunctional salicylate synthase, converts chorismate directly into salicylate, which is then activated by LusI, a putative AMP ligase (Fig. 3B). The activated salicylate then undergoes condensation with cysteine, catalyzed by the condensation/heterocyclization domain of the first NRPS module, LusQ, forming the initial thiazoline ring (**A** ring). This process is reminiscent of the biosynthesis observed in bacterial siderophores such as yersiniabactin [21] or piscibactin [19]. The ensuing PKS module – LusR – generates the olefin linkage by adding a malonate unit to the hydroxyphenyl-thiazoline, followed by reduction and dehydration through its KR and DH domains. The following NRPS modules LusS and LusT contain domains for cysteine incorporation and heterocycle formation. LusS also features an oxidation domain, consistent with the formation of the thiazole moiety (B ring), analogous to other thiazole-containing cyanobacterial natural products like aranazoles[22] and hectochlorin[23]. LusT, in addition to thiazoline formation (C ring), contains a SAM-dependent methyltransferase domain (cMT). LusU then carries out a PKS elongation, where malonyl is predicted as the substrate (AT domain contains the malonyl specific active site residue motifs GHSVG and HAFH), which is then fully reduced by its KR-DH-ER domains. This process results in the (methyl)ethyl linkage observed in the structure of lusichelins. However, bioinformatics analysis did not identify a methyltransferase domain within LusU, leaving the origin of the methyl group at C19 unclear. The final NRPS module, LusV, contains domains for the formation of the third thiazoline ring (D ring), and includes both cMT and type I thioesterase dom ains. LusY encodes a putative type II thioesterase as a standalone protein. Type I thioesterases typically release final products in NRPS/PKS biosynthesis, while type II thioesterases, when co-occurrent in the BGC, are often considered to have a "proofreading" role in the biosynthesis pathway.[24,25] This leads us to propose that LusV terminates the biosynthesis, resulting in the release of lusichelin C (**3**) (Fig. 3B). Moreover, compounds **1**, **2**, **4a** and **5a** contain a terminal methyl ester. The formation of the methyl ester **1** and **2** as artifacts of **3** during methanolic extraction was ruled out, as these compounds were also the major components when the extraction was performed with dichloromethane (SI Fig. S42-S43). We propose that this terminal methylation could be catalyzed by LusM, a putative SAM dependent methyltransferase with a leucine carboxyl methyltransferase (LCM) domain. Similar enzymatic functions have been reported in bacterial proteins such as StnF2 and MelK, which catalyze methyl esterification in the biosynthesis of streptonigrin[26] and melithiazol[27], respectively.

Lusichelins configuration analysis.

Due to limited compound availability, stereochemical studies were conducted exclusively with lusichelin C (**3**), which configuration was determined through a combination of *J*-based configurational analysis (JBCA), Electronic Circular Dichroism (ECD), TD-DFT calculations, and insights from the putative *lus* BGC.

The *Z* configuration of the Δ^{10} double bond of **3** was deduced from the characteristic $J_{H10\text{-}H11}$ value of 12 Hz (SI Table S1). The *syn* relative configuration between the C17 and C19 stereogenic centers in **3** was determined using the JBCA methodology. Firstly, $^{1}H\text{-}^{13}C$ heteronuclear coupling constant values were obtained via an HSQC-HECADE experiment (SI Fig. S24). Then, two rotamers around the C18/C19 bond were deduced from the *antiperiplanar* and *gauche* orientations between H18b/C24 and H18a/C24, suggested by the large and small heteronuclear coupling constants values of $^{3}J_{H18b\text{-}C24}$ (8.3 Hz) and $^{3}J_{H18a\text{-}C24}$ (1.2 Hz), respectively. Finally, the conformer **I** around the C18/C19 bond displayed in Fig. 4A was selected from the NOESY correlation between H18b and H19.

In the same way, the conformer **II** around the C17/C18 bond showed in Fig. 4A was deduced from the large and a small proton-proton coupling constant of 12.3 Hz and 4.5 Hz between H18b/H17 and H18a/H17, indicating an *antiperiplanar* and *gauche* disposition for these protons, respectively, along with NOESY correlation between H18a and H17.

Once the conformers **I** and **II** were deduced, *R** configuration was proposed for both stereogenic centers at C17 and C19 (Fig. 4B). This *syn* configuration between C17 and C19 agrees with the large $\Delta\delta_H$ value of 0.24 between chemical shifts of the two methylene diasterotopic protons at C18 following the geminal proton rule reported by Schmidt and Breis.[28]

The absolute configuration at C22 in **3** was determined using Marfey's analysis [28]. A careful derivatization of **3** was crucial to avoid the epimerization at the C_α of thiazoline ring under acidic or basic conditions [29]. For this reason, **3** was hydrolyzed in 1.5 M aqueous HCl at 90 ºC for 4 h and the resulting hydrolysate was derivatized with L-FDAA and analyzed by LC-MS.The presence of L -Cys in **3** was deduced from the comparison of the retention times and *m/z* values of the former hydrolysate derivative, analyzed by LC/MS, to those of L- and D-cysteine standards derivatized with L-FDAA. Specifically, the hydrolysate derivative of **3** exhibited a retention time (Rt) of 24.7 min and a *m/z* of 375, matching those obtained for the derivatized L-Cys standard (Rt of 25.03 min and *m/z* 375). In contrast, while the D-Cys standard derivatized displayed a *m/z* 375, its retention time (21.6 min) was clearly different (SI Fig. S26). Although the relative *syn* configuration between C17 and C19 and the absolute configuration at C22 could be determined in **3**, the absolute configuration of the stereogenic center at C9 could not be established. For this reason, four possible configurations (9*R*,17*R*,19*R*,22*R*, 9*S*,17*S*,19*S*,22*R*, 9*R*,17*S*,19*S*,22*R*, and 9*S*,17*R*,19*R*,22*R*) were considered and their corresponding ECD spectra were calculated using Time-Dependent Density Functional Theory (TD-DFT) at the CAM-B3LYP/6-311++G(2d,p) level, considering 50 electronic states. Comparison of the experimental ECD spectrum of **3** to those of the calculated

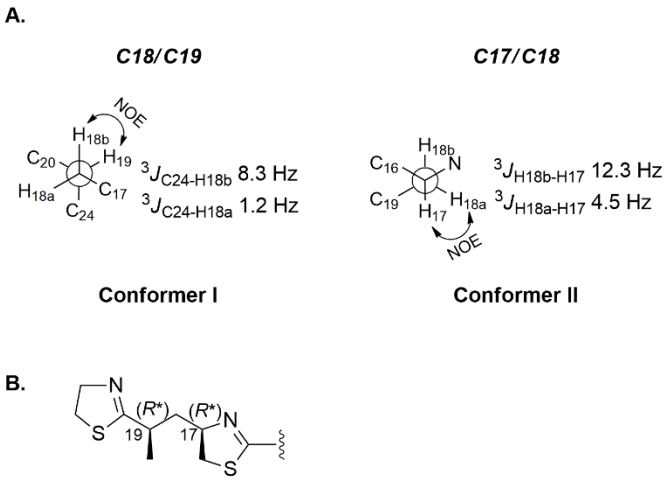

Fig. 4 (A) Newman projections of conformers **I** and **II** of **3**, around the C18-C19 and C17-C18 bonds, respectively, along with key experimental $^{3}J_{CH}$ and $^{3}J_{HH}$ coupling constants and NOESY correlations around these positions. **(B)** The *syn* relative configuration deduced between the stereogenic centers at C17 and C19 in **3**.

ones ruled out two of them, 9*S*,17*S*,19*S*,22*R* and 9*S*,17*R*,19*R*,22*R* (Fig. 5C and D). In contrast, the calculated DFT-ECD spectra for the remaining two (9*R*,17*S*,19*S*,22*R,* and 9*R*,17*R*,19*R*,22*R*) configurations matched very well to that of the experimental ECD spectrum of **3** (Fig. 5A and B). However, due to the high similarity of the ECD spectra, they cannot be distinguished, hence either 9*R*,17*S*,19*S*,22*R* or 9*R*,17*R*,19*R*,22*R* configurations are possible for **3**. (Fig. 5A and B). Bioinformatics analysis of the adenylation domains in modules LusQ, LusT, and LusV predicted L-cysteine as their substrate (SI Table S3), implying *R* configurations at the stereogenic centers C9, C17, and C22. No epimerase domains were identified in LusT and LusV, which would typically convert these centers to their D-configurations. Consequently, the 9*R* configuration was suggested for **3** and so, the 9*R*,17*R*,19*R*,22*R* absolute configuration is proposed for this compound as shown in Fig. 1. The relative configurations of lusichelins A-B (**1** and **2**) were further investigated by analyzing their NMR data. The small $\Delta\delta_H$ value of 0.08 between the proton chemical shifts of the diasterotopic H18 methylene protons in **1** is consistent with an *anti* C17/C19 relative configuration for these stereocenters following the geminal proton rule reported by Schmidt and Brei [30]. In this way, a *syn* C17/C19 relative configuration, as in **3**, was inferred from the large $\Delta\delta_H$ value of 0.51 between the H18 diasterotopic protons in **2**. This pattern was also observed in other natural products, including valactamides [31], verucopeptin [32], and polychlorinated leucine derivatives [33,34]. Unfortunately, further stereochemical studies on compounds **1** and **2** could not be conducted due to sample degradation, leaving their configurations undetermined. We hypothesize that **3** is the precursor to compounds **1** and **2**. Considering the configurational analysis, the configuration of **2** must be identical to that of **3**, specifically 9*R*,17*R*,19*R*,22*R* and so, the proposed configuration of **1** would be 9*R*,17*S*,19*R*,22*R*.

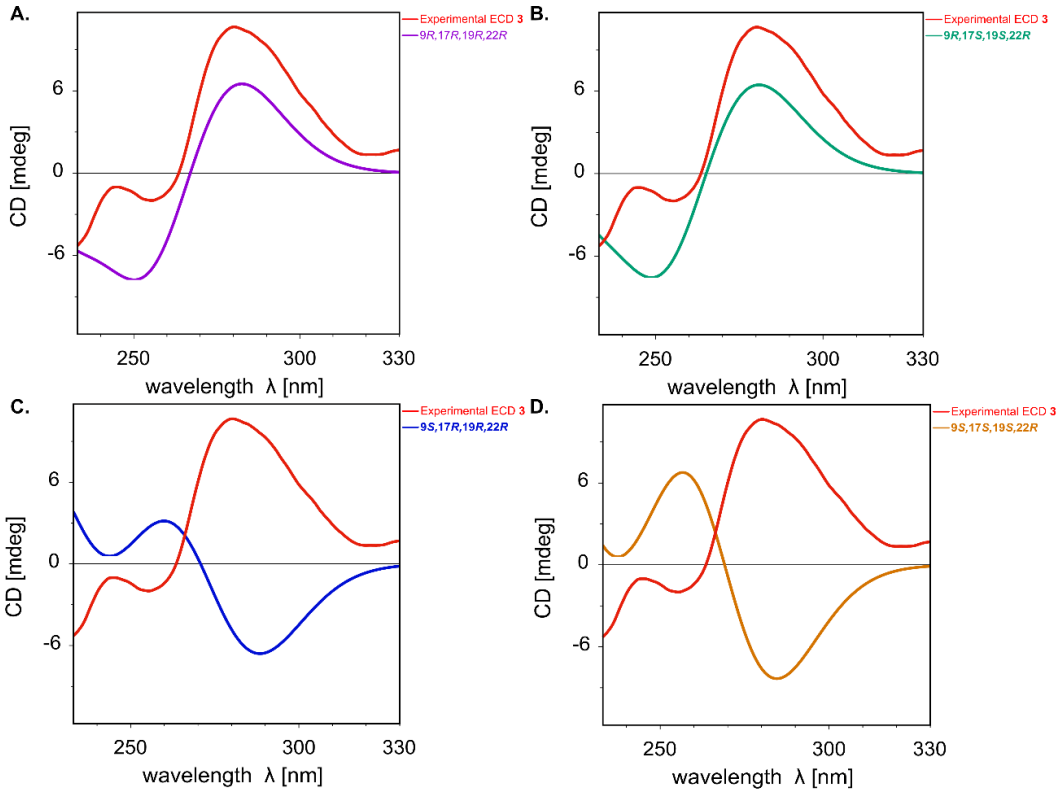

Fig. 5 (A) Comparison of the experimental ECD spectrum (red line) of lusichelin C (**3**) to the calculated TD-DFT ECD spectra for 9*R*,17*R*,19*R*,22*R* (violet line). **(B)** Comparison of the experimental spectrum (red line) compared to the calculated TD-DFT ECD spectra for 9*R*,17*S*,19*S*,22*R* (green line). **(C)** Comparison of the experimental spectrum (red line) compared to the calculated TD-DFT ECD spectra for 9*S*,17*R*,19*R*,22*R* (blue line). **(D)** Comparison of the experimental spectrum (red line) compared to the calculated TD-DFT ECD spectra for 9*S*,17*S*,19*S*,22*R* (yellow line).

Siderophore properties of lusichelin C (3). Compound **3** was also isolated from the biomass of *L. coriacea* LEGE 07167 as a complex with ferric iron (**3-Fe**, *m/z* $[M + Fe - 2H]^+$ = 597.9919; Δ = 52.9116). A proposed structure for **3-Fe** is shown in Fig. 6A where an octahedral complex is formed due to the presence of the appropriate ligands present in its framework: one thiazol and three thiazolines rings along with a phenolate and carboxylate groups.
The binding preference of *apo*-lusichelin C (**3**) for ferrous versus ferric iron was investigated. To assess this, **3** was incubated with equimolar amounts of $FeCl_2$ and $FeCl_3$, at three different pH values (Fig. 6B-D). At pH 6 and pH 8.5, the formation of the complex of **3** with Fe(III) was deduced from the overall increase in the UV-Vis spectral absorption, indicating a potential binding affinity to Fe(III) over Fe(II). The UV-Vis spectrum of this complex at pH 8.5 matched very well to that of the isolated Fe-lusichelin C (**3-Fe**), which corresponds to the pH of the culture medium (Fig. 6D).

Influence of iron deprivation and salt type on lusichelin production.

To investigate whether iron deficiency could regulate lusichelins production, cultures of *L. coriacea* LEGE 07167 were grown under iron deprived conditions using two types of salt: synthetic Tropic Marin® Pro-Reef (TM) sea salt (standard conditions) and ACS grade NaCl. The production of lusichelins A-C (**1-3**) was followed by LC-HRESIMS analysis of the culture media and biomass crudes (Fig. 7). It is worth noting that lusichelins A-B (**1-2**) were detected in higher concentrations in the cyanobacterial biomass compared to the culture media (Fig. 7A). This is likely due to their lipophilic nature (as compounds **1-2** have a calculated logP of 4.66 compared to 2.59 of **3**). Moreover, the type of salt had a more significant impact on lusichelins production than iron limitation. Cultures grown in TM (with or without Fe) produced approximately twice as much **1**-**3** as those grown in NaCl (with or without Fe) (Fig. 7A). These results suggest that iron limitation does not regulate the production of these compounds, which is atypical, as siderophore synthesis is usually upregulated under low iron conditions.[35] Further investigation into the expression of the AraC transcriptional regulator could provide more information about these compounds' regulatory mechanisms.

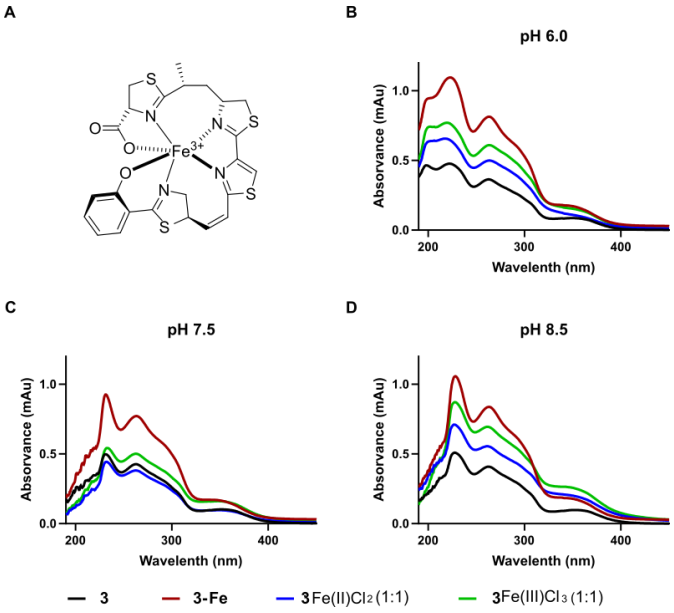

Fig. 6 (A) Proposed structure for the **3-Fe** complex. (B-D) UV–vis absorbance spectra at pH 6.0, 7.5 and 8.5: compound **3** (black line), its iron complex (**3-Fe**; red line), compound **3** incubated with equimolar amounts of ferric chloride (**3** : $Fe(III)Cl_3$; blue line) and ferrous chloride (**3**: $Fe(II)Cl_2$; green line).

Investigating other metallophore roles of lusichelins.

Copper plays a crucial role in cyanobacterial homeostasis, yet it is also a significant contributor to marine environmental pollution, primarily due to anthropogenic activities such as the use of copper in antifouling paints for ship hulls and as an algicide.[5] In a microcosm experiment, cyanobacteria were reported as the most copper-tolerant phylum among the prokaryotes found on marine periphytic biofilms exposed to environmentally relevant copper concentrations (0.01–10 µM).[36] To explore whether lusichelins could function as detoxifiers, cultures of *L. coriacea* LEGE 07167 were grown in Z8-NaCl media with elevated copper concentrations (200 and 450 nM Cu_2SO_4), which are 40 to 90 times higher than the typical copper concentration in Z8 medium (5 nM Cu_2SO_4). Under these conditions, a new complex was discovered in both biomass and culture media, compatible with a molecule of lusichelin C (**3**) bound to copper, as evidenced by an $[M+Cu-H]^+$ ion at *m/z* 605.9932 ($C_{24}H_{23}CuN_4O_3S_4$; Δ = -2.82 ppm). A comparative analysis of lusichelin production in 200 nM Cu_2SO_4 versus NaCl (5 nM Cu_2SO_4) revealed a clear recruitment of lusichelins to chelate copper in the culture media. This led to a significant reduction of apo-lusichelins in the biomass and their complete absence in the culture media (Fig. 7A). At 450 nM Cu_2SO_4, the abundance of the lusichelin-Cu complex (**3-Cu**) was significantly reduced (Fig. 7A), likely due to copper competing with other metals for their binding sites in metalloproteins, resulting in toxicity - a phenomenon previously observed for other cyanobacteria.[2] Surprisingly, new ions with the same protonated mass as lusichelin C (**3**), but with different retention times, were detected in the culture media (SI Fig. S44A). These ions were confirmed to cluster with lusichelins A-C (**1**-**3**) using a molecular network built in GNPS, indicating they share MS^2 fragmentation patterns and may represent putative isomers of lusichelin C (**3**) (SI Fig. S44B and C).

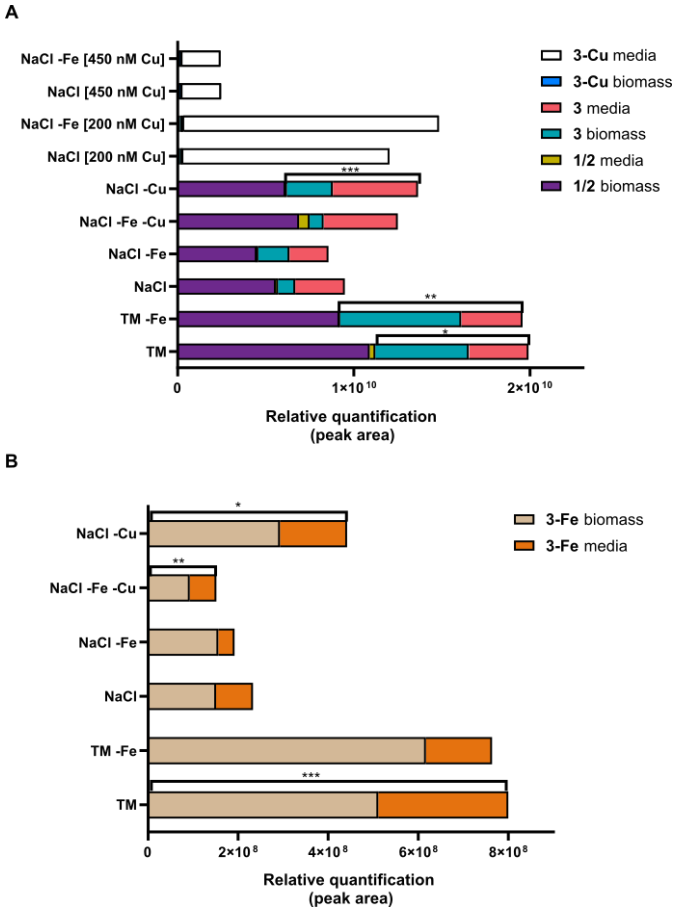

Fig. 7 Lusichelins production in response to: different salt sources (TM; NaCl); iron limitation (TM -Fe; NaCl -Fe); copper limitation (NaCl -Cu), dual metal restriction (NaCl -Fe -Cu); high copper concentration (NaCl [200 nM Cu]; NaCl [450 nM Cu]) and high copper concentration with iron restriction (NaCl -Fe [200 nM Cu]; NaCl -Fe [450 nM Cu]). Relative quantification in biomass and culture media was determined by the peak area of the extracted ion chromatogram for (**A**) lusichelins A-C (**1**-**3**) and copper-lusichelin C (**3**-**Cu**) complex; and (**B**) iron-lusichelin C (**3**-**Fe**) complex. The statistical differences (total amount of compound) of the different experimental conditions versus NaCl were tested using an unpaired t-test (*p ≤ 0.05; **p ≤ 0.01; ***p ≤ 0.001; n=3).

In cyanobacteria, copper and iron cooperate in some cellular processes, balancing their homeostasis as some Cu-binding and Fe-binding proteins can function interchangeably.[2,37] Thus, we investigated the effects on lusichelins production under conditions of copper restriction, dual restriction of iron and copper, and iron absence in cultures with excess copper. The absence of copper or dual restriction of both metals had no significant effect on the production of lusichelins A and B (**1** and **2**). However, there was a significant increase in compound **3** under copper deprivation, which was not observed for the dual restriction experiment (Fig. 7A). The Cu-lusichelin C (**3**) complex was not detected in any of these experimental conditions, while the Fe-lusichelin C (**3**) complex was twice as abundant in the copper restriction experiment (Fig. 7B). Cultures grown under iron restriction with excess copper (200 and 450 nM Cu_2SO_4) exhibited behavior similar to the experiments with copper excess alone, showing almost complete conversion of lusichelins to the Cu-lusichelin C (**3**) complex. The absence of iron did not significantly affect lusichelin production, and the iron complex was not detected in any of the copper-excess conditions (SI Fig. S44D). The role of lusichelins as metallophores appears to be more closely linked to copper homeostasis. Under high copper conditions, lusichelins likely function as detoxifiers, while copper absence seems to enhance the production of compound **3**. confirming the grouping of the new masses within the *apo*-lusichelins cluster. Each node depicts the distribution of each mass in the biomass and culture media. The putative new lusichelin C (**3**) isomers were only present in the culture media. (**D**) Molecular network cluster illustrating the metal-lusichelin complexes, demonstrating that the Fe-lusichelin C (**3-Fe**) complex is only detected in the control (NaCl), while the Cu-lusichelin C (**3-Cu**) complex is only detected in high copper concentration experiments.

Cytotoxic activity of lusichelins.

Our previous bioactivity-guided discovery study [17] identified *L. coriacea* LEGE 07167 as a promising source of novel cytotoxic compounds. To correlate the activity observed in the fractions with the pure compounds, we assessed the cytotoxicity of lusichelins against the same panel of human colon carcinoma HCT 116 cells using both monolayer (2D) and spheroid (3D) cell cultures. In the monolayer assay, compounds **2**, **3**, and **3-Fe** showed cytotoxicity with IC_{50} values of 1.16, 1.58, and 0.45 µM, respectively (Table S4). However, in the 3D cell cultures, only compound **2** retained the cytotoxicity (Table S4). Unlike 2D cultures, 3D tumor spheroids more closely mimic the physiology and structure of tumors, making them a more effective tool for screening potential anticancer candidates.[17] Due to their increased complexity, IC_{50} values in 3D models are typically at least four times higher than those observed in 2D cultures for other natural products.[38,39] Notably, compound **2**, the most potent compound in this study, differs from the inactive compound **1** only in the configuration of the stereocenter at C19, underscoring the critical role of stereochemistry in determining the bioactivity of these compounds.

The development of multidrug resistance (MDR) in cancer is a significant hurdle in treatment, often driven by the overexpression of P-glycoprotein (ABCB1).[40] This transmembrane protein, encoded by the *ABCB1* gene and a member of the ATP-binding cassette transporter family, functions as a broad-spectrum efflux pump, removing a wide range of chemotherapeutic drugs from cancer cells. Consequently, this reduces intracellular drug concentrations and promotes MDR. Therefore, compounds that can modulate or inhibit ABCB1 function represent promising strategies for overcoming MDR in cancer therapy.[41] Lusichelins were evaluated for their ability to reverse ABCB1-mediated MDR in mouse T-cell lymphoma L5178Y cells transfected with *ABCB1* (L5178Y-MDR) and their sensitive counterpart (L5178Y-PAR). Compounds **2**, **3**, and **3-Fe** exhibited comparable cytotoxicity against both cell lines, indicating a lack of selectivity for MDR phenotypes (Table S4). To further assess their effects, lusichelins were evaluated using the rhodamine-123 ABCB1 transport assay. Since ABCB1 actively transports rhodamine-123 out of cells, compounds that inhibit or modulate this process led to intracellular accumulation of the dye, indicating a potential reversal of MDR. Only compounds **1** and **2** reversed effectively the MDR phenotype at 2 µM, with fluorescence activity ratios (FAR) of 28 and 14.9, respectively. In comparison, tariquidar at 0.2 µM, the positive control, exhibited a FAR value of 98.2 (Fig. S45-47).

Conclusions

Natural products play a pivotal role in drug discovery and development, particularly in the treatment of cancer and infectious diseases.[42] However, since the 1990s, the pharmaceutical industry's interest in natural product research has declined owing to significant technical challenges, such as the frequent rediscovery of known molecules and the scarcity of natural products. Traditional biodiscovery approaches primarily relied on cell-based or target-based assays.[43] Nonetheless, recent advancements in analytical tools, genome mining, bioinformatics, and microbial culturing techniques have reignited interest in harnessing natural products for drug development.[43,44] Cyanobacteria, given their biosynthetic potential, are emerging as a promising source for discovering new secondary metabolites.[3,16] In our pursuit of anticancer compounds from cyanobacteria within our in-house culture collection (LEGE-CC), we combined advanced mass spectrometry metabolomics with robust cell-based assays.[17] As a result of this preliminary screening, this study successfully reports the discovery of lusichelins A-E (**1**-**5a**), a new group of bioactive metallophores isolated from the marine cyanobacterium *Lusitaniella coriacea* LEGE 07167. Despite structural similarities to bacterial salicyl-thiazol(in)e siderophores such as yersiniabactin[21], piscibactin[19], and pyochelin[45], lusichelins exhibit an unprecedented structural framework. Genome sequencing identified a putative BGC for lusichelins, encoding hybrid NRPS-PKS genes alongside signature genes indicative of metal-dependent regulation and transport, strongly suggesting their role as metallophores. Further investigation revealed that, rather than iron limitation, the type of salt used in the culture medium was the key factor influencing lusichelin production. The synthetic TM salt is rich in several trace elements that might be influencing the production of these compounds. Additionally, lusichelins function as copper detoxifiers, effectively chelating copper at high concentrations. These findings suggest that lusichelins may play a crucial role in cyanobacterial physiology and ecology by aiding in the acquisition of essential trace metals like iron while simultaneously providing protection against copper toxicity. This multifunctionality, recently reported for other cyanobacterial metallophores like leptochelins, highlights the versatility of these chelating molecules in adapting to metal fluctuations in the environment.[9] These discoveries raise new questions, particularly regarding the regulatory mechanisms involved in cyanobacterial metallophore production and the potential roles of these molecules in ecological interactions.

Beyond their metallophore properties, lusichelins, particularly lusichelin B (**2**), exhibit promising anticancer potential. Lusichelin B (**2**) demonstrated potent cytotoxicity against both monolayer cultures and tumor spheroids of human colon carcinoma HCT 116 cells, and it effectively overcame cancer MDR by modulating the efflux activity of the ABCB1 transmembrane pump.

The discovery of lusichelins as dual-function metallophores and anticancer agents expands our understanding of cyanobacterial secondary metabolism and highlights their potential as drug leads. These findings reinforce the continued relevance of natural products in modern drug discovery and open new avenues for developing innovative therapies.

Author contributions

MAR and MLS conceptualized the research. MLS, LF, DF, AMF, RCB, NS, GS, and MAR performed the experiments. MAR, GS, JR, and CJ supervised the research. MAR, PNL, VV, JR, and CJ acquired funding and provided resources. MLS and MAR wrote the original draft. All authors contributed to reviewing and editing the manuscript and approved the final version.

Conflicts of interest

There are no conflicts to declare.

Data availability

All experimental and characterization data, bioinformatics, mass spectrometry, NMR spectra and biological assays are available in the ESI. NMR data for 1–5 are also available at https://figshare.com/s/62d663132d004ecaf773.

Acknowledgements

This research was suported by the Portuguese Foundation for Science and Technology (FCT) within the scope of UIDB/04423/2020 and UIDP/04423/2020 and the WP9-Portuguese Blue Biobank under the Blue Economy Pact—Project N°. C644915664-00000026 co-funded by PRR, The Portuguese Republic, and the European Union.This project has also received funding from the European Union's Horizon 2020 research and innovation programme under grant agreement No 952374. The work was also supported by grant PID2021-122732OB- C22 from MCIN/AEI/10.13039/501100011033/ FEDER "A way to make Europe" (AEI, Spanish State Agency for Research and FEDER Programme from the European Union) and grant ED431C 2022/39 from Xunta de Galicia (Spain). G.S. was supported by the János Bolyai Research Scholarship (BO/00158/22/5) of the Hungarian Academy of Sciences. L.F. acknowledges the FCT grant 2022.11979.BD. RCB acknowledges the FCT grant SFRH/BD/136367/2018. D.F. thanks the BYT CIIMAR program for the BYT*plus* scholarship.

References

1 H. R. El-Seedi, M. F. El-Mallah, N. Yosri, M. Alajlani, C. Zhao, M. A. Mehmood, M. Du, H. Ullah, M. Daglia, Z. Guo, S. A. M. Khalifa and Q. Shou, *Mar. Drugs*, DOI:10.3390/md21080439.

2 M. J. Huertas, L. López-Maury, J. Giner-Lamia, A. M. Sánchez-Riego and F. J. Florencio, *Life*, 2014, **4**, 865–886.

3 J. Demay, C. Bernard, A. Reinhardt and B. Marie, *Mar. Drugs*, 2019, **17**, 1–49.

4 E. Årstøl and M. F. Hohmann-Marriott, *Mar. Drugs*, 2019, **17**, 281.

5 J. S. Cavet, G. P. M. Borrelly and N. J. Robinson, *FEMS Microbiol. Rev.*, 2003, **27**, 165–181.

6 J. Kramer, Ö. Özkaya and R. Kümmerli, *Nat. Rev. Microbiol.*, 2020, **18**, 152–163.

7 Y.-N. Ho, H.-J. Lee, C.-T. Hsieh, C.-C. Peng and Y.-L. Yang, in *Studies in Natural Products Chemistry*, Elsevier B.V., 1st edn., 2018, vol. 59, pp. 431–490.

8 G. W. Qiu, C. Koedooder, B. S. Qiu, Y. Shaked and N. Keren, *Trends Microbiol.*, 2022, **30**, 229–240.

9 N. E. Avalon, M. A. Reis, C. C. Thornburg, R. T. Williamson, D. Petras, A. T. Aron, G. F. Neuhaus, M. Al-Hindy, J. Mitrevska, L. Ferreira, J. Morais, Y. El Abiead, E. Glukhov, K. L. Alexander, F. A. Vulpanovici, M. J. Bertin, S. Whitner, H. Choi, G. Spengler, K. Blinov, A. M. Almohammadi, L. A. Shaala, W. R. Kew, L. Paša-Tolić, D. T. A. Youssef, P. C. Dorrestein, V. Vasconcelos, L. Gerwick, K. L. McPhail and W. H. Gerwick, *J. Am. Chem. Soc.*, 2024, **146**, 18626–18638.

10 S. J. Goldman, P. J. Lammers, M. S. Berman and J. Sanders Loehr, *J. Bacteriol.*, 1983, **156**, 1144–1150.

11 Y. Ito and A. Butler, *Limnol. Oceanogr.*, 2005, **50**, 1918–1923.

12 H. Beiderbeck, K. Taraz, H. Budzikiewicz and A. E. Walsby, *Zeitschrift fur Naturforsch. - Sect. C J. Biosci.*, 2000, **55**, 681–687.

13 T. Galica, N. Borbone, J. Mareš, A. Kust, A. Caso, G. Esposito, K. Saurav, J. Hájek, K. Řeháková, P. Urajová, V. Costantino and P. Hrouzek, *Appl. Environ. Microbiol.*, 2021, **87**, 1–13.

14 Z. L. Reitz and M. H. Medema, *Curr. Opin. Biotechnol.*, 2022, **77**, 102757.

15 K. Blin, S. Shaw, H. E. Augustijn, Z. L. Reitz, F. Biermann, M. Alanjary, A. Fetter, B. R. Terlouw, W. W. Metcalf, E. J. N. Helfrich, G. P. Van Wezel, M. H. Medema and T. Weber, *Nucleic Acids Res.*, 2023, **51**, W46–W50.

16 Y. Jeong, S. H. Cho, H. Lee, H. K. Choi, D. M. Kim, C. G. Lee, S. Cho and B. K. Cho, *Microorganisms*, 2020, **8**, 1–24.

17 L. Ferreira, J. Morais, M. Preto, R. Silva, R. Urbatzka, V. Vasconcelos and M. Reis, *Mar. Drugs*, 2021, **19**, 633.

18 A. T. Aron, E. C. Gentry, K. L. McPhail, L. F. Nothias, M. Nothias-Esposito, A. Bouslimani, D. Petras, J. M. Gauglitz, N. Sikora, F. Vargas, J. J. J. van der Hooft, M. Ernst, K. Bin Kang, C. M. Aceves, A. M. Caraballo-Rodríguez, I. Koester, K. C. Weldon, S. Bertrand, C. Roullier, K. Sun, R. M. Tehan, C. A. Boya P, M. H. Christian, M. Gutiérrez, A. M. Ulloa, J. A. Tejeda Mora, R. Mojica-Flores, J. Lakey-Beitia, V. Vásquez-Chaves, Y. Zhang, A. I. Calderón, N. Tayler, R. A. Keyzers, F. Tugizimana, N. Ndlovu, A. A. Aksenov, A. K. Jarmusch, R. Schmid, A. W. Truman, N. Bandeira, M. Wang and P. C. Dorrestein, *Nat. Protoc.*, 2020, **15**, 1954–1991.

19 A. Souto, M. A. Montaos, A. J. Rivas, M. Balado, C. R. Osorio, J. Rodríguez, M. L. Lemos and C. Jiménez, *European J. Org. Chem.*, 2012, 5693–5700.

20 T. Steinmetz, W. Hiller and M. Nett, *Beilstein J. Org. Chem.*, 2022, **18**, 360–367.

21 D. A. Miller, L. Luo, N. Hillson, T. A. Keating and C. T. Walsh, *Chem. Biol.*, 2002, **9**, 333–344.
22 P. Moosmann, R. Ueoka, M. Gugger and J. Piel, *Org. Lett.*, 2018, **20**, 5238–5241.
23 A. V. Ramaswamy, C. M. Sorrels and W. H. Gerwick, *J. Nat. Prod.*, 2007, **70**, 1977–1986.
24 R. F. Little and C. Hertweck, *Nat. Prod. Rep.*, 2022, **39**, 163–205.
25 S. I. Ohlemacher, Y. Xu, D. L. Kober, M. Malik, J. C. Nix, T. J. Brett and J. P. Henderson, *J. Biol. Chem.*, 2018, **293**, 19572–19585.
26 F. Xu, D. Kong, X. He, Z. Zhang, M. Han, X. Xie, P. Wang, H. Cheng, M. Tao, L. Zhang, Z. Deng and S. Lin, *J. Am. Chem. Soc.*, 2013, **135**, 1739–1748.
27 S. Weinig, H.-J. Hecht, T. Mahmud and R. Müller, *Chem. Biol.*, 2003, **10**, 939–952.
28 K. Harada, K. Fujii, T. Mayumi, Y. Hibino, M. Suzuki, Y. Ikai and H. Oka, *Tetrahedron Lett.*, 1995, **36**, 1515–1518.
29 P. Wipf and P. C. Fritch, *J. Am. Chem. Soc.*, 1996, **118**, 12358–12367.
30 Y. Schmidt and B. Breit, *Org. Lett.*, 2010, **12**, 2218–2221.
31 T. Zhang, J. Feng, H. Oikawa, Y. Guo and T. Ye, *Precis. Chem.*, 2024, **2**, 120–126.
32 A. Yoshimura, S. Kishimoto, S. Nishimura, S. Otsuka, Y. Sakai, A. Hattori and H. Kakeya, *J. Org. Chem.*, 2014, **79**, 6858–6867.
33 A. Ardá, C. Jiménez and J. Rodríguez, *Tetrahedron Lett.*, 2004, **45**, 3241–3243.
34 A. Ardá, C. Jiménez and J. Rodríguez, *European J. Org. Chem.*, 2006, 3645–3651.
35 E. V. Soares, *Appl. Microbiol. Biotechnol.*, 2022, **106**, 3985–4004.
36 N. Corcoll, J. Yang, T. Backhaus, X. Zhang and K. M. Eriksson, *Front. Microbiol.*, 2019, **10**, 1–15.
37 Z. H. Zhen, S. Qin, Q. M. Ren, Y. Wang, Y. Y. Ma and Y. C. Wang, *Front. Bioeng. Biotechnol.*, 2021, **9**, 1–13.
38 M. L. Sousa, M. Preto, V. Vasconcelos, S. Linder and R. Urbatzka, *Front. Oncol.*, 2019, **9**, 1–13.
39 M. L. Sousa, T. Ribeiro, V. Vasconcelos, S. Linder and R. Urbatzka, *Toxicon*, 2020, **175**, 49–56.
40 K. Engle and G. Kumar, *Eur. J. Med. Chem.*, 2022, **239**, 114542.
41 J. Dong, L. Yuan, C. Hu, X. Cheng and J. J. Qin, *Pharmacol. Ther.*, 2023, **249**, 108488.
42 D. J. Newman and G. M. Cragg, *J. Nat. Prod.*, 2020, **83**, 770–803.
43 A. G. Atanasov, S. B. Zotchev, V. M. Dirsch, I. E. Orhan, M. Banach, J. M. Rollinger, D. Barreca, W. Weckwerth, R. Bauer, E. A. Bayer, M. Majeed, A. Bishayee, V. Bochkov, G. K. Bonn, N. Braidy, F. Bucar, A. Cifuentes, G. D'Onofrio, M. Bodkin, M. Diederich, A. T. Dinkova-Kostova, T. Efferth, K. El Bairi, N. Arkells, T. P. Fan, B. L. Fiebich, M. Freissmuth, M. I. Georgiev, S. Gibbons, K. M. Godfrey, C. W. Gruber, J. Heer, L. A. Huber, E. Ibanez, A. Kijjoa, A. K. Kiss, A. Lu, F. A. Macias, M. J. S. Miller, A. Mocan, R. Müller, F. Nicoletti, G. Perry, V. Pittalà, L. Rastrelli, M. Ristow, G. L. Russo, A. S. Silva, D. Schuster, H. Sheridan, K. Skalicka-Woźniak, L. Skaltsounis, E. Sobarzo-Sánchez, D. S. Bredt, H. Stuppner, A. Sureda, N. T. Tzvetkov, R. A. Vacca, B. B. Aggarwal, M. Battino, F. Giampieri, M. Wink, J. L. Wolfender, J. Xiao, A. W. K. Yeung, G. Lizard, M. A. Popp, M. Heinrich, I. Berindan-Neagoe, M. Stadler, M. Daglia, R. Verpoorte and C. T. Supuran, *Nat. Rev. Drug Discov.*, 2021, **20**, 200–216.
44 K. Scherlach and C. Hertweck, *Nat. Commun.*, 2021, **12**, 1–12.
45 C. D. Cox, K. L. Rinehart, M. L. Moore and J. C. Cook, *Proc. Natl. Acad. Sci. U. S. A.*, 1981, **78**, 4256–4260.